Effect of cross-field drifts on flows in the main scrape-off-layer of DIII-D L-mode plasmas

2009 Nucl. Fusion 49 115002

(http://iopscience.iop.org/0029-5515/49/11/115002)

Nucl. Fusion **49** (2009) 115002 (14pp) doi:10.1088/0029-5515/49/11/115002

Effect of cross-field drifts on flows in the main scrape-off-layer of DIII-D L-mode plasmas

M. Groth[1], J.A. Boedo[2], N.H. Brooks[3], R.C. Isler[4], A.W. Leonard[3], G.D. Porter[1], J.G. Watkins[5], W.P. West[3], B.D. Bray[3], M.E. Fenstermacher[1], R.J. Groebner[3], R.A. Moyer[2], D.L. Rudakov[2], J.H. Yu[2] and L. Zeng[6]

[1]Lawrence Livermore National Laboratory, PO Box 808, Livermore, CA 94551, USA
[2] University of California San Diego, La Jolla, CA 92093, USA
[3] General Atomics, PO Box 85608, San Diego, CA 92186-5608, USA
[4] Oak Ridge National Laboratory, Oak Ridge, TN 37831, USA
[5] Sandia National Laboratory, PO Box 5800, Albuquerque, NM 87185 USA
[6] University of California Los Angeles, Los Angeles, CA 90095, USA

Received 30 January 2009, accepted for publication 5 August 2009
Published 11 September 2009
Online at stacks.iop.org/NF/49/115002

Abstract
The flow velocities of deuterons and low charge-state carbon ions have been measured simultaneously in the main scrape-off-layer (SOL) in low-density plasmas in DIII-D, and the dependences of these flow fields on the direction of the cross-field drifts ($\boldsymbol{E} \times \boldsymbol{B}$ and $\boldsymbol{B} \times \nabla B$) have been investigated. These measurements were taken poloidally localized in the SOL region vertically opposite the divertor X-point. The carbon ion flows do not necessarily match those of the deuterons either in the direction with respect to the magnetic field lines or in magnitude, suggesting that physics effects apart from entrainment play a significant role in the impurity response. In configurations with the ion $\boldsymbol{B} \times \nabla B$ drift towards the divertor X-point, the parallel-$\boldsymbol{B}$ deuteron velocities at the plasma crown are high (-20 to $-30\,\mathrm{km\,s^{-1}}$ in the direction of the high field side (HFS) divertor), while they are nearly zero in configurations with the opposite $\boldsymbol{B} \times \nabla B$ drift direction. The flow direction of singly and doubly charged carbon ions is independent of the ion $\boldsymbol{B} \times \nabla B$ drift direction, and the ions flow at approximately -5 to $-10\,\mathrm{km\,s^{-1}}$ towards the HFS divertor. Simulations with the UEDGE code have been carried out to better understand the underlying physics processes. Inclusion of cross-field drifts in the simulations produced divertor solutions for density and temperature that agree significantly better with measured divertor parameters. These simulations do not, however, reproduce the measured flow fields at the crown for the configuration with the ion $\boldsymbol{B} \times \nabla B$ drift towards the divertor X-point. The UEDGE code has also been used to understand the influence of pumping at the HFS divertor plate, and a poloidal dependence in the radial transport coefficient.

PACS numbers: 52.30.Ex, 52.65.Kj, 52.40.Hf, 52.55.Fa

(Some figures in this article are in colour only in the electronic version)

1. Introduction

Flows in the scrape-off-layer (SOL) of tokamak plasmas play a critical role in the long-range migration of eroded materials from the main chamber and divertor surfaces to their final locations of net deposition ([1, 2] and references therein). In tokamaks with carbon-based plasma-facing components (PFCs), these flows may enable carbon sputtered from the main chamber walls to migrate to the divertor chamber where it forms hydrogen-rich carbon layers on the divertor surfaces. Since these films do not saturate in thickness, a tritium inventory may build up which could potentially limit the duty cycle of future, long-pulse fusion devices, such as ITER [3, 4]. Understanding the SOL flow pattern and its impact on material migration may permit development of mitigation techniques for tritium accumulation in ITER and other future fusion devices. Plasma flows in the main SOL and private flux region (PFR) also affect the degree of divertor detachment [5], which influences the effectiveness of volumetric radiation and divertor compression of impurities [6] to mitigate divertor target head loads, and of divertor pumping to control core density.

This paper describes simultaneous flow measurements of deuteron and low-charge state carbon ions parallel to the magnetic field, $\boldsymbol{B}$, in the SOL of low-density, low-confinement (L-mode) plasmas in DIII-D. The flows were measured in single-null (SN) configurations in the plasma region vertically opposite the divertor X-point, approximately midway poloidally between the high field side (HFS) and the low field side (LFS) of the magnetic axis. In the context of this paper, we define this region as the 'crown' of the plasma. This paper focuses exclusively on measurements and their comparison with numerical simulations at the crown, with the emphasis on the relationship between deuteron and carbon transport processes. Measurements of the deuteron flow at the LFS equatorial plane in DIII-D will be published elsewhere. L-mode confinement was chosen as the simplest plasma condition to study, because edge-localized modes (ELMs) do not perturb the SOL and the low input power of L-modes permit reciprocating Langmuir probe measurements of the deuteron flow. The experimental results obtained in L-mode may not be directly translated to high-confinement (H-mode) plasmas, as ELMs modulate the recycling sources and SOL pressure distribution, and thus the SOL flow field. Because of significantly higher heat fluxes to the Langmuir probe head associated with H-mode, probes measurements in H-mode plasmas are scarce. Using L-mode plasmas, on the other hand, represents a tractable problem for both detailed measurements and SOL simulations. Building confidence that the simulations capture all the essential physics in simple L-mode plasma, they can then be used to simulate the SOL of H-mode plasmas.

Unique to this study, the parallel-$\boldsymbol{B}$ velocities of low charge-state carbon ions (C^{1+}, C^{2+}) were inferred at similar poloidal locations as those of the deuterons using passive Doppler spectroscopy [7] and the poloidal C^{1+} velocity from two-dimensional (2D) imaging [8]. Measuring both species at the same poloidal location permits a direct assessment of the degree of entrainment of carbon ions in the deuteron flow. Although it has been previously asserted that SOL impurities of low atomic number are sufficiently entrained in the deuteron flow to explain the carbon deposition profiles measured in trace-C^{13} experiments ([2] and references therein), experimental proof has been lacking.

Measurements of the deuteron flow at the crown in other tokamaks show a strong dependence of the flows on the ion $\boldsymbol{B} \times \nabla B$ drift direction [9, 10], but no systematic studies of carbon SOL flows have been published. In previous studies of SN configurations with the ion $\boldsymbol{B} \times \nabla B$ drift towards the divertor X-point, the deuteron flow reaches near-sonic flow velocities (parallel Mach number, $M_\parallel \sim -0.5$ to -1.0) in the direction of the HFS divertor at the crown, while in those with the ion $\boldsymbol{B} \times \nabla B$ drift away from the X-point, the SOL flow stagnates at the crown [4]. (A more complete review of the measured SOL flow pattern in tokamaks can be found in [11].) Interpretation of carbon plume images in methane injection experiments in Alcator C-mod [12] and DIII-D [13] with OEDGE code simulations [14] was consistent with low charge-state carbon ions flowing along with the deuterons at approximately $M_\parallel \sim -0.4$ along the magnetic field lines in the direction of the HFS divertor. In this study on DIII-D, the effect of cross-field drifts on the SOL flows was investigated experimentally by reversing the toroidal magnetic field, B_T, while keeping the direction of the plasma current constant.

Although simulations with 2D multi-fluid, edge modelling codes can predict many of the measured plasma parameters in the main and divertor SOL to within a factor of 2 [15–17], reproducing the direction and magnitude of the flow pattern in the main SOL has remained one of the most challenging tasks in edge modelling [18–24]. Recent studies with the EDGE2/NIMBUS and SOLPS codes identified that the low plasma flow observed in the simulations is related to underestimating the radial electric field in the SOL [24, 25]. Simulations with the fluid edge code UEDGE [26] showed qualitatively and quantitatively the same result: the simulated flow velocities of the deuterons and low charge-state carbon ions are significantly lower than their measurements [27]. Consequently, numerical studies of trace C^{13} injection into the main SOL at the crown of a DIII-D L-mode plasma with UEDGE predicted that C^{13} is predominately deposited at the LFS target plate (90% to LFS and <10% to HFS) [8]. Experimentally, C^{13} was found to be deposited mainly on the HFS target [28]. By including the cross-field drift terms due to $\boldsymbol{B} \times \nabla B$ and $\boldsymbol{E} \times \boldsymbol{B}$ in the simulations, the numerical solutions for the divertor plasma parameters come into significantly better agreement with measurements [17]. They do not, however, improve the agreement of the measured and predicted SOL flow pattern at the crown, nor the C^{13} deposition pattern at the divertor targets [8]. In this paper the numerical studies presented in [8, 27] are expanded, including the dependence of the calculated flows in the main SOL on magnetic field direction, and variations in the assumed transport model and boundary conditions.

2. Measurement of deuteron and carbon flow velocities at the crown

2.1. Experimental arrangement

The flow velocities of deuterons and low charge-state carbon ions were measured in diverted L-mode plasmas at low core plasma density, i.e. 20–25% of the Greenwald density [29]. Upper single-null (USN) configurations were employed to enable flow measurements in the crown with the comprehensive diagnostic systems installed in the lower divertor of the DIII-D vessel (figure 1). Typical discharge parameters were plasma current, $I_P = 1.1$ MA, toroidal field, $B_T = 2.0$ T, edge safety factor $q_{95} = 4.5$, volume-averaged density, $\langle n \rangle_{vol} = 2 - 2.5 \times 10^{19}$ m^{-3} and total heating power, $P_{tot} = 1.0$–1.3 MW. The plasma current was kept in the same direction when the toroidal field was reversed: it was in the same direction as the toroidal field in the configuration with the ion $\boldsymbol{B} \times \nabla B$ drift towards the divertor X-point (USN-$V_{\nabla B\uparrow}$). These discharges are also characterized by the absence of active pumping in the divertor; passive pumping by the walls constitutes the only particle sink. At the separatrix on the LFS midplane, the measured plasma parameters were $n_e \sim (7$–$10) \times 10^{18}$ m^{-3}; $T_e \sim 50$–70 eV and $T_i \sim 150$–200 eV, resulting in electron and ion collisionalities, ν_e^* and ν_i^*, of approximately 5 and 0.5, respectively. These measurements were accomplished with a multi-point Thomson scattering system [30], a reciprocating probe [31] and a charge exchange

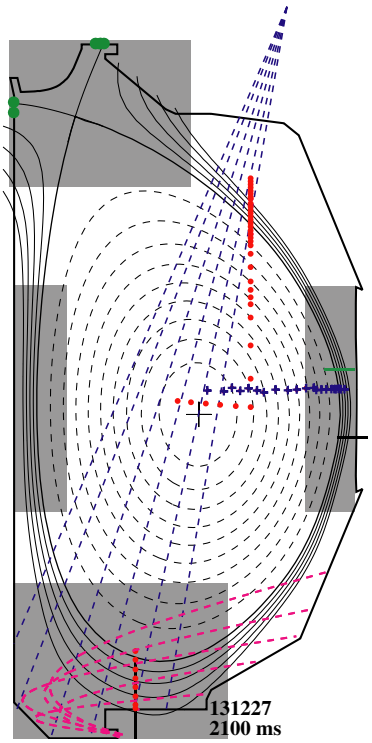

Figure 1. USN plasma configuration with overlays of principle diagnostics used in this study: divertor X-point and LFS midplane reciprocating Langmuir probes (black solid lines), vertical and tangential multi-chord divertor spectrometer (dashed blue lines, dashed-magenta), tangential divertor and midplane cameras (grey boxes). Other diagnostics include core and divertor Thomson scattering system (red dots), CER spectroscopy (blue crosses), reflectometer (green solid line) and upper divertor Langmuir probes (green dots).

recombination (CER) system [32], all three systems being installed at the LFS equatorial plane (figure 1). The SOL is, therefore, expected to be marginally collisional for the electrons and collisionless for the ions. Consequently, the SOL ion flow is sheath-limited. In such low-collisionality regimes, the divertor strike points are predicted to be well attached to the target plates [33]. Imaging of carbon emission from the divertor confirmed that the LFS strike point is attached to the plate; however, the HFS divertor plasma is significantly colder than 5 eV and detached in the immediate vicinity of the separatrix. Without externally applied torque, toroidal rotation measurements of fully stripped carbon ions with the CER system indicate that the core plasma rotates in the co-current direction at approximately 15 to 20 km s^{-1} at a normalized poloidal flux, Ψ_N, of 0.8. At the separatrix the toroidal velocity is lower, about 5 km s^{-1}. These plasma conditions were held constant during the 3.5 s long density flattop, midway through which methane was injected in toroidally symmetric fashion for 1.5 s, at a rate of $\sim$1 Pa m^3 s^{-1}, to enhance the carbon emission on the HFS of the crown for line-filtered imaging. The injection led to a factor-of-two increase in carbon emission on the LFS of the crown and, concomitantly, to a 10–20% increase in $\langle n \rangle_{vol}$ and in the SOL total radiated power. Comparison of the measured, parallel-$\boldsymbol{B}$ flow velocities of the deuterons, C^+ and C^{2+}, prior and during the methane injection showed that the injection did not affect the flow velocities.

The principal flow diagnostics at the crown of the plasma are a reciprocating, multi-tipped Langmuir probe [34] for the parallel-$\boldsymbol{B}$ deuteron flow, a high-resolution spectrometer [35] for line emission measurements along quasi-tangentially viewing chords for the parallel-$\boldsymbol{B}$ C^{1+} and C^{2+} velocities, and a set of tangentially viewing cameras [36] for the poloidal C^+ velocity (figure 1). The parallel- $\boldsymbol{B}$ Mach number ($M_\parallel$) of the deuteron flow is measured on the HFS of the crown. It is calculated from the ratio of the ion saturation currents at the electron and ion sides, j^e_{sat} and j^i_{sat}, using Hutchinson's formula [37]: $M_\parallel = \alpha \ln(j^e_{sat}/j^i_{sat})$, where α depends on the SOL collisionality and 0.4 was assumed in this study [38]. Using the measured electron densities and temperatures along the probe reciprocation path, and assuming equilibrated electron and ion temperatures ($T_e = T_i$), the absolute deuteron speed can be determined: $v_\parallel = M_\parallel \cdot (2kT_e/m_d)^{1/2}$. The parameter m_d is the deuteron mass. The thereby yielded deuteron velocity represents an upper limit. Assuming T_i in the range of 3–5 times T_e, as it was measured for similar SOL plasma parameters in Tore Supra and other tokamaks [39], the deuteron flow velocity could be a factor 1.4–1.7 lower than by adopting electron/ion equipartition. The carbon ion flow speeds were deduced from spectroscopic analysis of the Doppler shifts in the C II doublet (2P–2S) at 658 nm and the C III triplet (3P–3S) at 465 nm [7]; the unshifted line profiles on vertical chords were used to deduce absolute wavelength references for interpreting the shift along the quasi-tangential chords. The dependence of magnetic splitting on field strength along the tangential views was used to localize the C^{1+} and C^{2+} emission zones.

Imaging of the emission from successive dissociation and ionization stages of the methane break-up process during the injection into the crown was used to estimate the order-of-magnitude poloidal velocity of C^{1+} ions. The poloidal velocity of carbon ions was calculated from the poloidal shifts of the emission peaks and ionization time due to electron impact (equation (1) from [8]). For this estimation to have validity, the excitation time of the electronic transition must be comparable to the ionization time to the next charge state. Since the emission increase was visible at the HFS of the crown only, the poloidal velocity of C^{1+} can only be estimated in this region. Other diagnostics used in this study include a second multi-point Thomson system spanning the core and SOL regions at the LFS [40], a reflectometer system at the LFS midplane [41] and a set of Langmuir probes embedded in the LFS and HFS divertor plates [42] (figure 1).

2.2. Effect of toroidal field direction on the measured SOL flows at the crown

The parallel-$\boldsymbol{B}$ velocity of the deuterons strongly depends on the direction of the ion $\boldsymbol{B} \times \nabla B$ drift, while the parallel-$\boldsymbol{B}$ velocities of singly and doubly charged carbon ions are nearly independent of the drift direction (table 1 figures 2–4). In the configuration with the ion $\boldsymbol{B} \times \nabla B$ drift towards the divertor X-point (USN-$V_{\nabla B\uparrow}$) the deuterons flow towards the HFS divertor at approximately one-half of the local ion sound speed ($V_{\parallel,D+} \sim -20$ km s^{-1}), while in the case with the ion $\boldsymbol{B} \times \nabla B$ drift away from the divertor X-point (USN-$V_{\nabla B\downarrow}$) the deuteron flow at the crown is almost stagnant (figure 10(a), from [43]). Negative velocities and Mach numbers denote

Table 1. Deuteron and low charge-state carbon ion flow velocities obtained at the crown in low-density L-mode plasmas. Negative flow velocities denote flow towards the HFS divertor plate.

	USN-$V_{\nabla B\uparrow}$	USN-$V_{\nabla B\downarrow}$
$M_{\|\|}^{D^+}$	Crown HFS: -0.5	$\sim$Zero
$v_{\|\|}^{D^+}$ (km s^{-1}) (w/$T_e = T_i$)	-15 to -35 km s^{-1}	
$V_{\|\|}^{C1^+}$ (km s^{-1})	Crown HFS: -5 to -7	HFS: -6 to -8
$V_{pol}^{C1^+}$(km s^{-1})	Crown HFS: -0.2 to -0.3	HFS: -0.2 to -0.3
$V_{\|\|}^{C2+}$ (km s^{-1})	Crown HFS: -5 to -10	HFS: -10 to -15

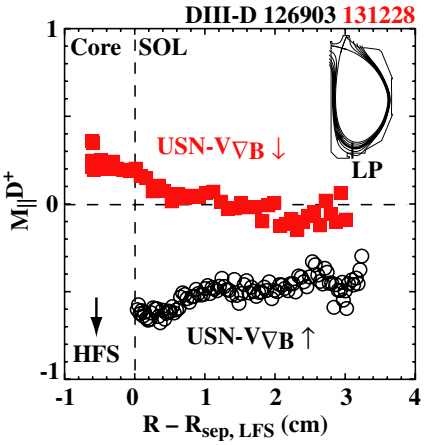

Figure 2. Parallel-B flow velocities of deuterons at the HFS of the crown measured in plasmas with the ion $\boldsymbol{B} \times \nabla B$ drift towards (USN-$V_{\nabla B\uparrow}$, black open circles, DIII-D discharge 126903) and away from the divertor X-point (USN-$V_{\nabla B\downarrow}$, red solid squares, DIII-D discharge 131228). The deuteron velocities are expressed by the Mach number and plotted as a function of distance from the separatrix measured at the LFS midplane, $R - R_{sep,LFS}$. Positive Mach numbers denote flow towards the LFS divertor. The inset shows the magnetic configuration and the reciprocating path of the divertor Langmuir probe.

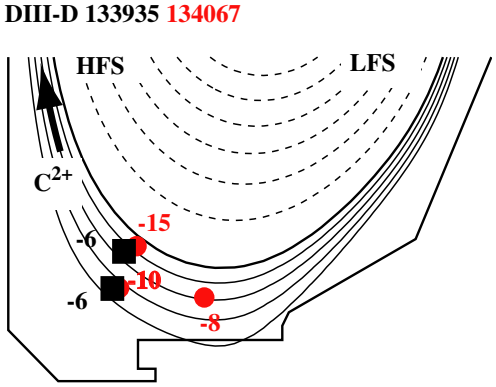

Figure 3. Parallel-$\boldsymbol{B}$ C^{2+} ion velocities, in units of (km s^{-1}), at the measurement locations in the USN-$V_{\nabla B\uparrow}$ (DIII-D shot 133935, black squares) and USN-$V_{\nabla B\downarrow}$ (DIII-D shot 134067, red circles) magnetic configurations. Positive velocities correspond to flow counter-clockwise with respect to the magnetic axis.

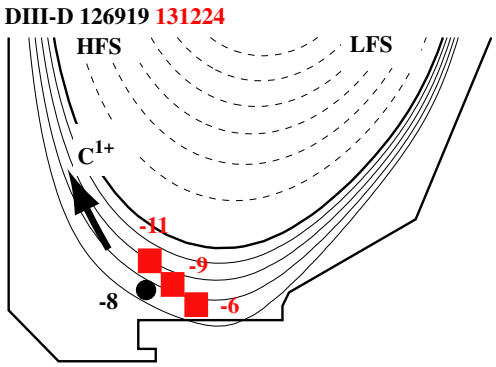

Figure 4. Parallel-$\boldsymbol{B}$ C^{1+} ion velocities, in units of (km s^{-1}), at the measurement locations in the USN-$V_{\nabla B\uparrow}$ (DIII-D shot 126919, black squares) and USN-$V_{\nabla B\downarrow}$ (DIII-D shot 131224, red circles) magnetic configurations.

motion towards the HFS divertor. Toroidally, deuteron flow is in the direction of the plasma current (co-current). Poloidally, the deuteron flow was measured in the HFS of the crown. For the USN-$V_{\nabla B\uparrow}$ configuration, the $\boldsymbol{E}_r \times \boldsymbol{B}$ component of the poloidal flow is in the opposite direction to the poloidal flow derived from the measured parallel-$\boldsymbol{B}$ flow, while for the USN-$V_{\nabla B\downarrow}$ configuration the $\boldsymbol{E}_r \times \boldsymbol{B}$ flow is in the same direction. In the USN-$V_{\nabla B\uparrow}$ case, the deuteron flow decreases monotonically from a value of $V_{\|,D^+} \sim -35$ km s^{-1} near the separatrix to ~ -15 km s^{-1} in the far SOL. In the USN-$V_{\nabla B\downarrow}$ configuration, $M_{\|} \sim +0.1$ ($v_{\|} \sim +5$ km s^{-1}) towards the LFS divertor adjacent to the separatrix, reversing to $M_{\|} \sim -0.1$ ($v_{\|} \sim -0.5$ km s^{-1}) towards the HFS divertor in the far SOL. The uncertainty of the deuteron flow measurements based on discharge-to-discharge comparison is of the order 0.1 to 0.2 for the Mach number and 0.5 to 5 km s^{-1} for the deuteron flow velocity. The obtained deuteron Mach speeds are similar in direction and absolute speeds to those obtained near the crown in JET Ohmic plasmas [9]. The radial resolution is of the order 5 mm in real space or 1 mm with respect to the distance from the separatrix at the LFS midplane.

Doubly charged carbon ions, C^{2+}, were measured to flow parallel to $\boldsymbol{B}$ towards the HFS divertor on the HFS of the crown (figure 3). The absolute magnitude of the measured C^{2+} flow velocities is -5 to -15 km s^{-1}, with a fall-off by a factor 2 to 5 with radial distance from the separatrix. The largest uncertainty in the carbon ion velocity measurements is introduced via the spectral analysis; typically, the uncertainty is of the order 1–2 km s^{-1}. Spatially, the uncertainty of the measurement location is of the order 2–3 cm in real space and 1 cm in LFS midplane equivalent. The magnitudes of the C^{2+} flow velocities were a factor of 2 to 3 lower in the USN-$V_{\nabla B\uparrow}$ configuration than in the USN-$V_{\nabla B\downarrow}$ case. Singly charged carbon ions, C^{1+}, were previously measured at the HFS of the crown for both ion ∇B cases to flow along $\boldsymbol{B}$ towards the HFS divertor at velocities at -5 to -10 km s^{-1} (figure 4) (USN-$V_{\nabla B\uparrow}$ case shown in [27]), consistent with both the previous and the more recent results for C^{2+}. The

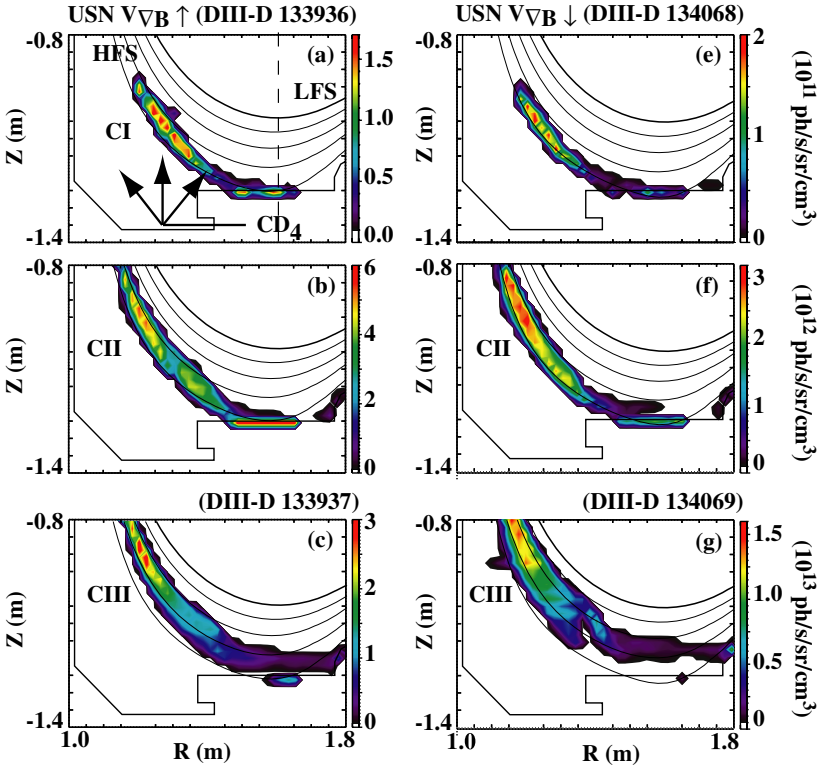

Figure 5. Tomographic reconstructions of the C I 910 nm ((*a*) and (*d*)), C II 516 nm ((*b*) and (*e*)) and C III 465 nm ((*c*) and (*f*)) emission profiles during the methane injection. The left-hand column (*a*)−(*c*) shows the intensity distributions in plasmas for the USN-$V_{\nabla B\uparrow}$ (DIII-D shot 133936 and 133937), the right-hand column (*d*)−(*f*) for the USN-$V_{\nabla B\downarrow}$ case (DIII-D shot 134068 and 134069). The dashed vertical line in (*a*) indicates the partition between HFS and LFS of the crown.

measured, parallel-$\boldsymbol{B}$ flow velocities of the deuterons in the HFS of the crown, and C^+ and C^{2+} in the HFS and LFS of the crown, prior and during the methane injection are the same within the uncertainty of the measurements.

Although collisional entrainment of the carbon ions in the background deuteron flow may explain the measured carbon flow direction and speed in the USN-$V_{\nabla B\uparrow}$ configuration, the results obtained in the USN-$V_{\nabla B\downarrow}$ case are inconsistent with such an explanation. In the USN-$V_{\nabla B\uparrow}$ configuration the C^{2+} velocity on the HFS of the crown is a factor of 2 lower than the deuteron velocity, but in the same direction. A full explanation is further complicated by the fact that the carbon flow locations in the crown are slightly displaced poloidally to the HFS and LFS from those of the deuteron flow measurements. In addition, entrainment in the deuteron flow along $\boldsymbol{B}$ depends on how the electrostatic collision rates between the deuterons and carbon ions compare with loss rates of the carbon ions by ionization, recombination and perpendicular transport. The Spitzer stopping time, τ_s, for electrostatic collisions between C^+ and D^+ [44] is of the order 50 μs, only one-half of the electron impact ionization time, τ_{ioniz}, for the transition from C^+ to C^{2+}. Experimental data from the reciprocating probe and divertor Thomson scattering were used to estimate these time constants. Higher charge-state carbon ions couple more efficiently to the deuteron flow, because τ_s decreases with charge state Z, as $1/Z^2$. For C^{2+} (C^{3+}) ions, for example, the Spitzer stopping time is 50 (100) times shorter than the ionization time to the next higher charge state.

During methane injection into the HFS of the crown, the centroids of the poloidal emission profiles, for the hydrocarbon fragment CD and successive ionization stages of the carbon atoms, shift progressively towards the HFS divertor (figure 5). Using the poloidal distance between the centroids of the C I, C II and C III emission profiles as shown in figure 5, and the ionization time calculated from the local SOL plasma conditions, a poloidal C^{1+} velocity of −200 to −300 m s^{-1} can be deduced from the images. The direction and magnitude of this inferred poloidal C^{1+} flow velocity, along with the pitch angles of the total magnetic field determined by EFIT equilibrium reconstruction [45] are consistent with a poloidal projection of the purely parallel-$\boldsymbol{B}$ motion towards the HFS divertor in the HFS of the crown measured by Doppler spectroscopy ($V_{\parallel,C^+} \sim -8\,\mathrm{km\,s^{-1}}$, $|\boldsymbol{B}|/B_{\mathrm{pol}} \sim 27$, thus $V_{\mathrm{pol},\parallel,C^+} \sim -300\,\mathrm{m\,s^{-1}}$).

Comparison of the CD (431 nm), C I, C II and C III poloidal intensity distributions does not show a discernable dependence on the ion $\boldsymbol{B}\times\nabla B$ drift direction (figure 5). Since the parallel-$\boldsymbol{B}$ velocities of C^{1+} and the local plasma conditions at the crown are almost identical for the two $\boldsymbol{B}\times\nabla B$ drift cases, the inferred poloidal velocity of C^{1+} ions is estimated to be of the same magnitude and therefore independent of the toroidal field direction.

The estimated magnitude of $\boldsymbol{E}_r\times\boldsymbol{B}$ drift velocity ($v_{E\times B}$) of C^+ at the HFS of the crown, on the other hand, is of the same order as the poloidal projection of the parallel-$\boldsymbol{B}$ velocity. The radial electric field, $\boldsymbol{E}_r$, was derived from measurements with the reciprocating Langmuir probe of T_e and the floating potential, V_f, assuming for the plasma potential, V_p, $3.5kT_e+V_f$ [38] (USN-$V_{\nabla B\uparrow}$: figure 6). At the flux surface at which the

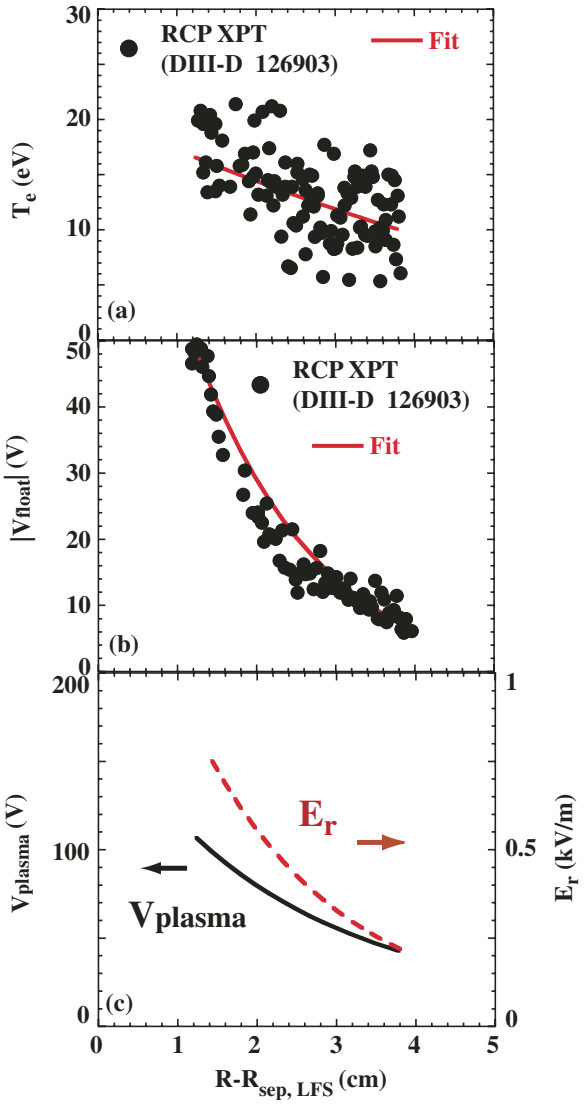

Figure 6. Radial profiles of the measured (solid symbols) and fitted (solid lines) electron temperature (*a*) and floating potential (*b*) and the derived plasma potential (black solid) and electric field (red dashed) (*c*) for the USN-$V_{\nabla B\uparrow}$ configuration (DIII-D shot 126903). The electron temperatures and floating potentials (symbols) were measured with the reciprocating probe at the crown.

C II emission peaks, $\boldsymbol{E}_r$ is about 300 V m^{-1} in the USN-$V_{\nabla B\uparrow}$ configuration, thus $v_{E\times B}$ is approximately +150 m s^{-1} in the direction of the LFS divertor. For the USN-$V_{\nabla B\downarrow}$ case, $\boldsymbol{E}_r$ is larger than in USN-$V_{\nabla B\uparrow}$, about 500 V m^{-1}, thus $v_{E\times B} \sim -250$ m s^{-1} towards the HFS divertor. Consequently, since the C^+ parallel-$\boldsymbol{B}$ velocities are of similar magnitude for the two $\boldsymbol{B}\times\nabla B$ drift cases (figure 4), one would expect to observe a difference in the poloidal shifts between C I and C II. However, such poloidal shifts were not seen in the carbon emission profiles. An independent and more accurate measurement of the carbon poloidal flow velocity is needed to clarify the apparent discrepancy of the above measurements.

Further evidence of preferential transport of the injected carbon ions from the HFS of the crown to the HFS divertor comes from the relative brightness of the C II and C III emission in the images of the HFS and LFS midplane regions taken with tangentially viewing cameras (figure 7 for CIII). In the HFS of the SOL just below the midplane the emission at both wavelengths increased roughly fourfold when methane is injected, while only a 10% to 15% increase was observed at the LFS midplane. Since the electron density and temperature in the HFS and LFS midplane SOL can be assumed constant during the methane injection, the increase in the carbon emission is mainly due to an increase in the carbon ion density.

3. Predictive SOL Simulations with UEDGE

SOL flows were studied numerically with the 2D multi-fluid edge code UEDGE [26], including cross-field drift terms due to $\boldsymbol{E}\times\boldsymbol{B}$ and $\boldsymbol{B}\times\nabla B$ [46]. In UEDGE, plasma transport in the $\boldsymbol{B}$ direction is modelled using the fluid Bragiinski equations, including kinetic corrections. Flux limits were used in the parallel particle and energy transport equations to account for kinetic effects due to the low ion collisionality in the main SOL ($\nu_i^* \sim 0.5$). Perpendicular to $\boldsymbol{B}$, transport was assumed to be purely diffusive, and modelled with radially varying transport coefficients to match the measured LFS midplane profiles of n_e, T_e and T_i (figure 8). To study the effect of poloidal variations in the radial transport, a set of simulations were run with a poloidal dependence of the transport coefficients as an inverse function of the toroidal magnetic field (e.g. $1/B_T$, $1/B_T^2$, etc). These equations are solved on a non-orthogonal grid derived from EFIT equilibrium reconstructions, which span core, edge and SOL regions between Ψ_N of 0.9 and 1.09 ($R - R_{sep,LFS}$ between –4 cm and +4 cm, respectively). The parameter $R - R_{sep,LFS}$ is the distance from the separatrix measured at the LFS midplane. The toroidal field vector was run forward and reverse to simulate the plasma in cases with the ion $\boldsymbol{B}\times\nabla B$ towards and away from the X-point, respectively. Plasma rotation was imposed as a boundary condition at the UEDGE core boundary by specifying the toroidal momentum. Deuterons striking the divertor target plates, the grid boundary facing the PFR and the outermost grid boundary in the main SOL are recycled with 100% efficiency, whereas deuterium neutrals are recycled with 100% efficiency at the target plates and with 99% at the outermost grid boundary. Carbon released by physical and chemical sputtering at the plates and by chemical sputtering at the walls is injected using published rates [47] into the computational domain as neutral atoms. Its transport is modelled using a force balance equation in the parallel-$\boldsymbol{B}$ direction [48], and diffusion in the radial direction with the same transport coefficients as for the deuterons, and collisional ionization and recombination rates are from ADAS [49]. The total toroidal momentum is defined at the UEDGE core boundary to match the measured core rotation of fully stripped carbon ions. Here, a toroidal momentum of $+1 \times 10^{-2}$ N m s in the co-current direction was assumed yielding toroidal velocities of 15 km s^{-1} at Ψ_N of 0.9. For a limited set of UEDGE cases, carbon was injected at the HFS of the crown at trace level (10^{19} C atoms) to simulate the injection of methane. The injection of methane cannot be simulated with the current UEDGE version, since the code does not have the capability of handling hydrocarbon molecules.

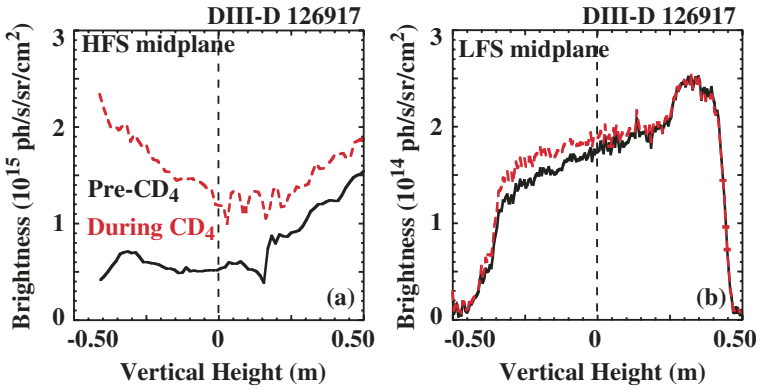

Figure 7. Vertical emission profiles of C III 465 nm emission in the midplane regions of (*a*) the HFS and (*b*) the LFS (DIII-D shot 126917). Note the order-of-magnitude difference in vertical scales! Data are shown for times prior to and during methane injection (black solid and red dashed lines, respectively).

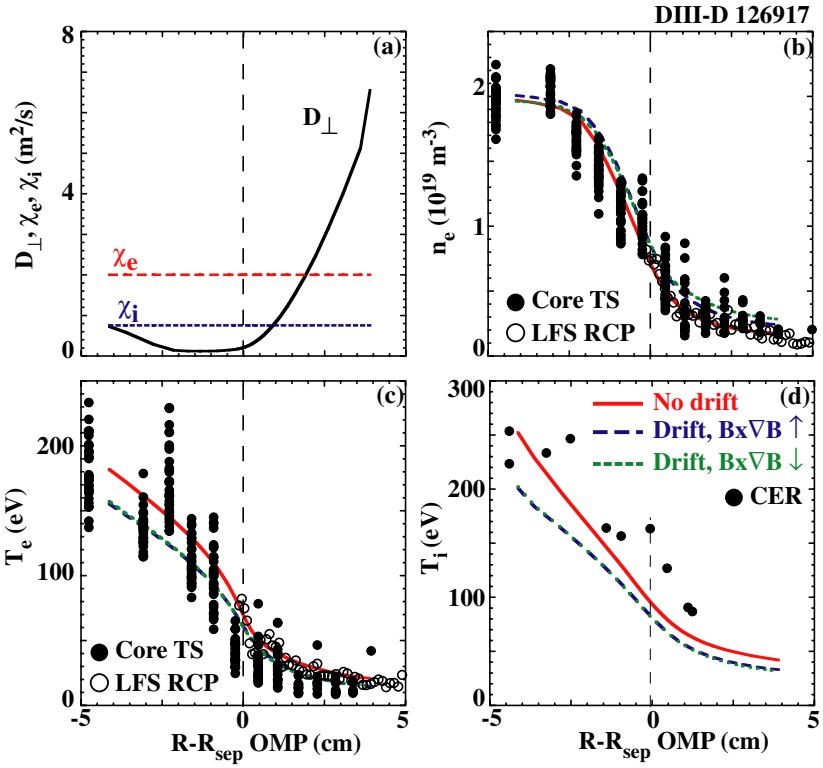

Figure 8. (*a*) Radial profiles of the radial transport coefficients, (*b*) electron density, (*c*) electron temperature and (*d*) ion temperature. The experimental data (DIII-D shot 126917, circles) were measured by core Thomson scattering, core TS and LFS reciprocating Langmuir probe, LFS RCP (*b*), (*c*) and CER spectroscopy (*d*). Predictions from UEDGE simulations are shown for cases with the cross-field drifts for USN-$V_{\nabla B\uparrow}$ (dashed blue line) and USN-$V_{\nabla B\downarrow}$ (dotted green line) and the case without drifts (solid red line).

3.1. Effect of cross-field drifts and toroidal field direction on the simulated SOL flows

The magnitude of the predicted deuteron Mach number at the crown is low for both ion ∇B drift directions. For the USN $V_{\nabla B\uparrow}$ configuration the calculated Mach number is significantly lower than the measured Mach number, while low deuteron flow is predicted by UEDGE for the USN-$V_{\nabla B\downarrow}$ case, in agreement with the measurements (figures 2 and 9). The predicted Mach number is derived from the predicted electron and ion temperatures at the crown that UEDGE calculates independently from the Bragiinski energy equations. Using the predicted electron temperature only, and assuming $T_\mathrm{i} = T_\mathrm{e}$ as for the Langmuir probe measurements, the calculated Mach number is approximately 20% higher than in the case using the actual predicted T_e and T_i. The direction and magnitude of the simulated deuteron flows at the crown is qualitatively similar to numerical results obtained with the EDGE2D and SOLPS codes for a JET Ohmic plasma [18, 24]. Inclusion of the $\boldsymbol{E}\times\boldsymbol{B}$ and $\boldsymbol{B}\times\nabla B$ drift terms in the UEDGE simulations of the USN-$V_{\nabla B\uparrow}$ case did not significantly change the direction and magnitude of the deuteron flow (figure 9) at the crown as explained below. It did, however, result in solutions of the divertor plasma that are in significantly better agreement with

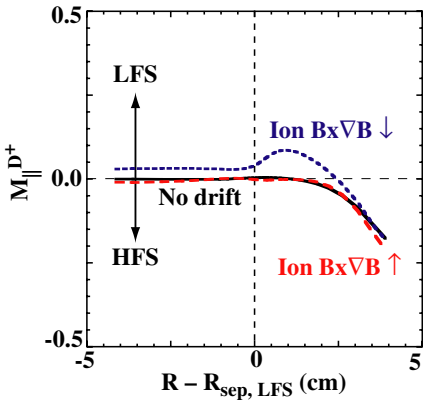

Figure 9. Predicted parallel-$\boldsymbol{B}$ deuteron flow at the crown as a function of the distance from the separatrix, $R - R_{\mathrm{sep,LFS}}$, for UEDGE cases with the drift terms for both directions of the ion $\boldsymbol{B} \times \nabla B$ drifts (red dashed and blue dotted) and the case without drift terms (black solid). The experimental data are shown in figure 2.

the measurements. With the drift terms included, the electron temperature at the HFS plate near the separatrix decreases from 20 to 2 eV, making the calculated divertor plasma more consistent with Langmuir probe measurements of the ion flux to the target, and carbon emission profile measurements in the divertor (figure 10). The simulated electron temperature at the LFS strike zone does not change significantly; however, the simulated C III emission becomes more localized at the strike point when the drift terms are included. These observations are consistent with earlier findings, for example in JET [15] and DIII-D [16, 17, 50]. They were attributed to $\boldsymbol{E} \times \boldsymbol{B}$ driven plasma flow from the outer strike zone to the inner strike zone across the PFR region, which depletes the outer strike zone and increases the plasma density at the inner strike zone. While the C III emission was measured near the X-point in the HFS divertor plasma, suggesting that the divertor plasma at the HFS strike point is significantly colder than 2 eV [51], the simulation with the drift terms included still predicts C III emission at the HFS strike zone. The simulation indicates that the HFS divertor is on the threshold of detaching from the HFS target plate, although detachment at the HFS strike point ($T_{\mathrm{e}} < 2$ eV) has not been obtained within the series of UEDGE runs.

The UEDGE simulations predict that the deuteron flow along the magnetic field lines is driven by the pressure gradient between the divertor X-point and the crown produced by (1) recycling in the divertor, (2) $\boldsymbol{E} \times \boldsymbol{B}$ driven flow in the PFR [50] and (3) ion $\boldsymbol{B} \times \nabla B$ drifts across the separatrix at the crown and the divertor X-point, when the cross-field drifts are included (figure 11). This flow pattern is offset by radial fluxes across the separatrix, peaking at the LFS midplane region. In both $\boldsymbol{B} \times \nabla B$ drift directions, a stagnation point is formed near the crown, with its exact poloidal location depending on (1)–(3). In the USN-$V_{\nabla B\uparrow}$ case, the radial particle flux across the separatrix at the crown is from the SOL into the core plasma domain reducing the plasma pressure in this region: the total flow in the HFS and LFS main SOL is predominately towards the crown. In the USN-$V_{\nabla B\downarrow}$ configuration, the $\boldsymbol{B} \times \nabla B$ driven flux at the crown is from the core into the SOL producing a pressure peak at the crown: the flow in the HFS and LFS main SOL is away from the crown. The simulated flow pattern in the

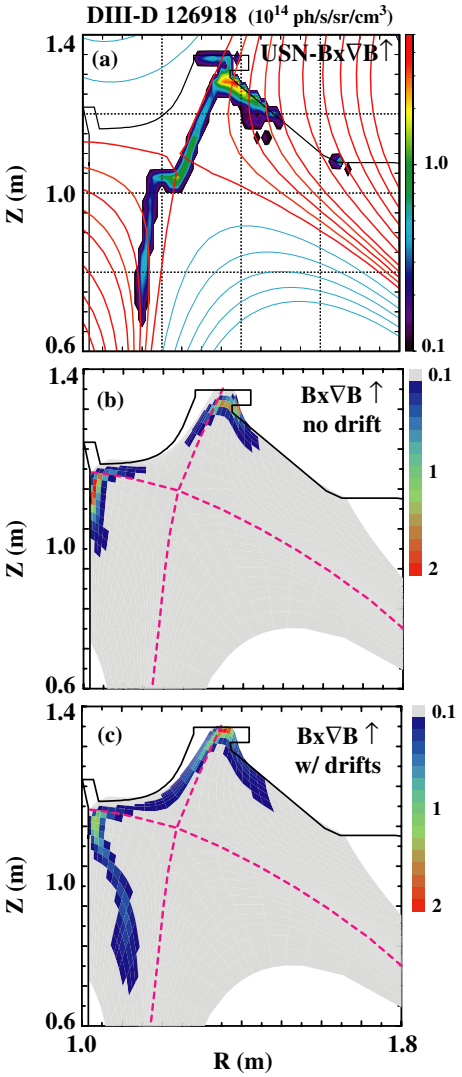

Figure 10. Poloidal profiles of C III 465 nm emission in the upper divertor. Panel (*a*) shows the experimental profile measured by a tangentially viewing camera (DIII-D shot 126918), (*b*) the UEDGE prediction for a simulation not including cross-field drifts and (*c*) the UEDGE prediction with the cross-field drifts included in the USN-$V_{\nabla B\uparrow}$ configuration.

main SOL at the LFS midplane is consistent with ion Pfirsch–Schlüter return currents previously measured by Asakura *et al* [52] and Pitts *et al* [53] in the JT60-U and TCV tokamaks, respectively. These return currents have also been observed numerically in EDGE2D and SOLPS simulations [20, 54]. Detailed measurements and simulations of the SOL parallel-B deuteron flow at the LFS midplane in DIII-D will be presented in a separate publication.

Poloidally, the UEDGE simulations show that the $\boldsymbol{E} \times \boldsymbol{B}$ driven flow can be of equal magnitude to the poloidal projection of the parallel flow, or even dominate the flow pattern. At the crown, the $\boldsymbol{E} \times \boldsymbol{B}$ component is the dominant flow component at the separatrix, since the UEDGE-calculated radial electric field is strongest (figure 12). Measurements of the radial electric field, $\boldsymbol{E}_r$, in the SOL at the crown with the reciprocating Langmuir probe indicate that the $\boldsymbol{E} \times \boldsymbol{B}$ driven flow is larger than the UEDGE predicted flow: the simulated $\boldsymbol{E}_r$

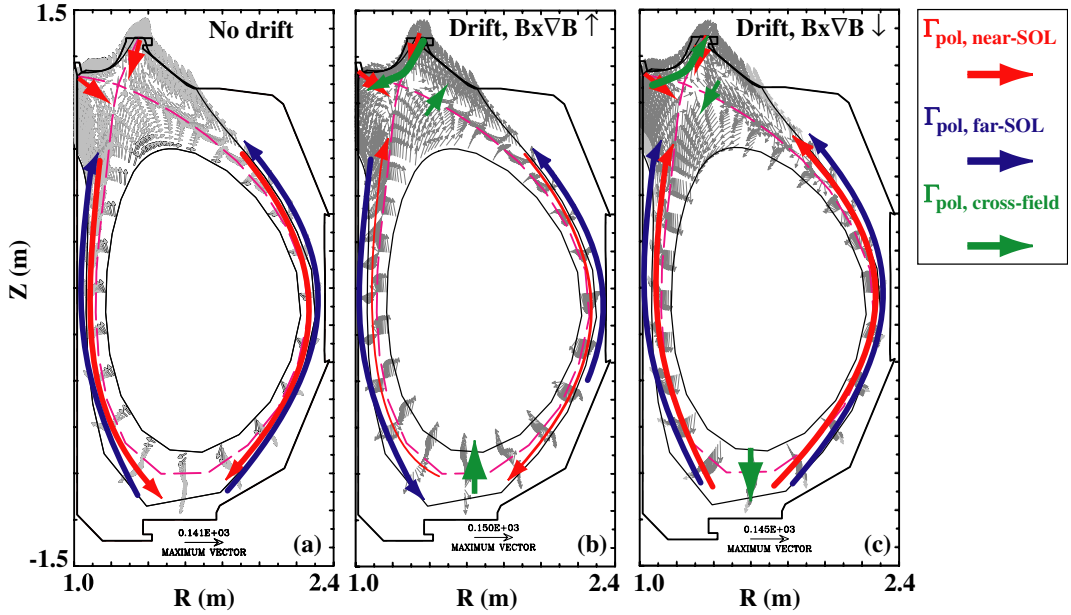

Figure 11. Predicted poloidal flow pattern of deuterons in the main and divertor SOL and in the core. UEDGE simulations for cases (*a*) without drifts, (*b*) with cross-field drifts and the ion $\boldsymbol{B} \times \nabla B$ drift towards the divertor X-point and (*c*) with cross-field drifts and the ion $\boldsymbol{B} \times \nabla B$ drift away from the divertor X-point. The arrows are colour-coded for flows due to plasma motion along $\boldsymbol{B}$ in the near-separatrix (red) and far SOL (blue) regions, and flows due to cross-field drifts (green, $\boldsymbol{E} \times \boldsymbol{B}$ and $\boldsymbol{B} \times \nabla B$).

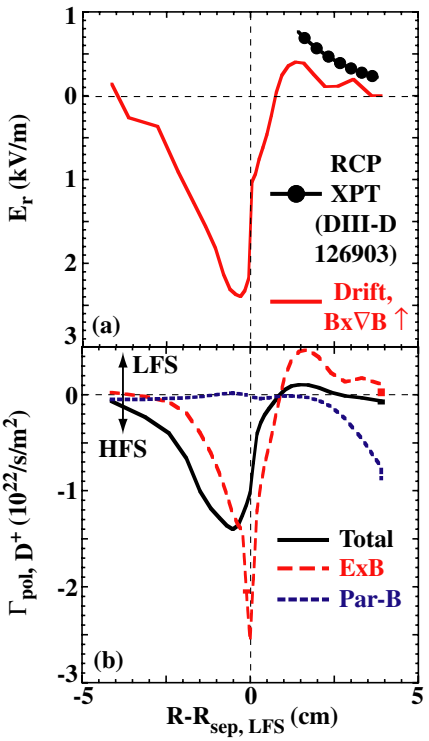

Figure 12. (*a*) Radial electric field at the crown as calculated from the divertor X-point probe data (DIII-D shot 126903, black dotted line) and predicted by UEDGE including cross-field drifts (red solid line). (*b*) The poloidal flux of D^+ ions separated in total (black solid line), $\boldsymbol{E} \times \boldsymbol{B}$ (red dashed) and parallel projection from the parallel flow (blue dotted).

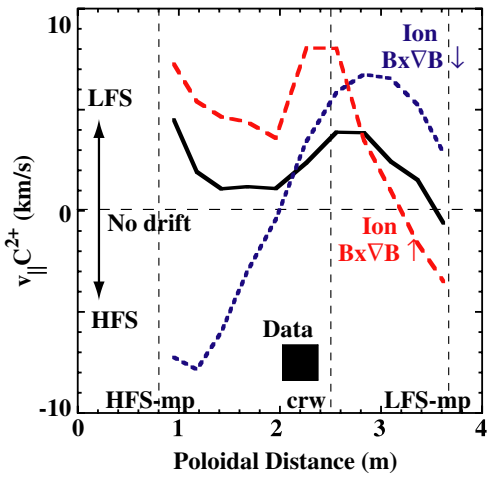

Figure 13. Calculated parallel-$\boldsymbol{B}$ C^{2+} flow velocities as a function of poloidal distance from the HFS (1 m) to the LFS (3.6 m) midplane for the flux surface at distance 2 cm at the outer midplane. The grid cell representing the tip of the crown is indicated by the vertical dashed line at 2.5 m. The experimental data for the HFS (solid square) are replicated from figure 3. The UEDGE case without drift terms is shown by the black solid line; the case with drift terms is shown in red dashed line for USN-$V_{\nabla B\uparrow}$ and in blue dotted line for USN-$V_{\nabla B\downarrow}$.

near the separatrix is approximately a factor of 2 lower than the measured $\boldsymbol{E}_r$. The plasma potential and the radial electric field that were derived in this study are similar to those previously measured for DIII-D [38]. The simulations also show that the radial electric field is negative in the SOL near the separatrix, and positive in the far SOL (figure 12(*a*)), thus in the USN-$V_{\nabla B\uparrow}$ configuration, the poloidal $\boldsymbol{E} \times \boldsymbol{B}$ driven flow is towards the HFS divertor in the near-separatrix region and towards the LFS divertor in the far SOL region (figure 12(*b*)). The direction of these flows changes sign with the reversal of B_T.

In the USN-$V_{\nabla B\uparrow}$ case, the predicted parallel-$\boldsymbol{B}$ velocity of C^{2+} at the HFS and LFS of the crown is in the direction of the LFS divertor in disagreement with the measured velocity

(figure 13). With the drifts included the C^{2+} flow velocity increases at the HFS and decreases at the LFS of the crown, and flow reversal occurs halfway between the crown and the outer midplane. In the USN-$V_{\nabla B\downarrow}$ configuration, C^{2+} ions also flow in the direction of the LFS divertor at the LFS of the crown, at comparable flow velocities as in the USN-$V_{\nabla B\uparrow}$ case. However, the simulation produces a stagnation point at the HFS of the crown, and the C^{2+} flow in that region is towards the HFS divertor.

The UEDGE simulations indicate that transport of C^{2+} ions at and near the crown is determined by the balance between the frictional drag force exerted by the deuterons and the ion temperature gradient (∇T_i) force produced by the background plasma [48]:

$$F_\mathrm{fric} = m_{C^{2+}} \frac{(v_{D^+} - v_{C^{2+}})}{\tau_\mathrm{s}}, \tag{1}$$

$$F_{\nabla T_\mathrm{i}} = \beta \nabla T_{i,\parallel}, \tag{2}$$

where τ_s is the Spitzer stopping time, β is a coefficient depending on the charge of the impurity ion and masses of the deuteron and impurity ions (here, $\beta \approx 10$). Forces due to the existence of an ion pressure gradient (∇p_i) and an electron temperature gradient (∇T_e) along $\boldsymbol{B}$ [48] are also calculated by UEDGE. In the main SOL, including the crown, these forces are significantly weaker than the frictional drag and the ∇T_i force. In the following discussion, the ∇p_i and ∇T_e forces are therefore neglected.

In the simulations of the USN-$V_{\nabla B\uparrow}$ configuration, the simulated ion temperature in the main SOL is highest at the LFS midplane region, and falls off towards both divertor plates (figure 14(*a*)). At the crown the predicted ion temperature profile is consistent with spectroscopic measurements of the C^{2+} ion temperatures, also shown in figure 14(*a*), indicating the existence of a poloidal gradient in the direction of the midplane. It results in a ∇T_i force that accelerates C^{2+} ions in the direction of the LFS divertor from the HFS to the LFS midplane until the drag force produced by the velocity difference between the deuterons and C^{2+} matches the ∇T_i force (figure 14(*c*)). At the crown the absolute magnitude of the simulated flow velocity of the deuterons is significantly lower than that of C^{2+} ions (figure 14(*b*)). Consequently, the drag force decelerates C^{2+} ions in the direction of the HFS divertor (figure 14(*c*)). Incidentally, the velocity difference as calculated by UEDGE ($\Delta v \sim 10\,\mathrm{km\,s^{-1}}$) is of the same order of magnitude as the measured velocity difference ($\Delta v \sim 15\,\mathrm{km\,s^{-1}}$). Assuming that the velocity difference remains the same, an increase in the deuteron flow towards the HFS divertor would consequently result in a flow of C^{2+} ions also in the direction of the HFS divertor. The ratio of the drag over the ∇T_i force may be used to assess the combined effect of the two forces. The net force is generally zero since the drag and ∇T_i forces are of almost the same value but opposite direction. At the tip of the crown, the ratio as calculated by UEDGE is of the order unity, hence the forces are essentially in balance and C^{2+} ions are transported in the direction of the LFS divertor (figure 14(*d*)). The experimental data, on the other hand, suggest the force ratio to be of the order 2, which would force C^{2+} to flow towards the HFS divertor. The discrepancy between the experimental data and the simulations is mainly the result of significantly higher

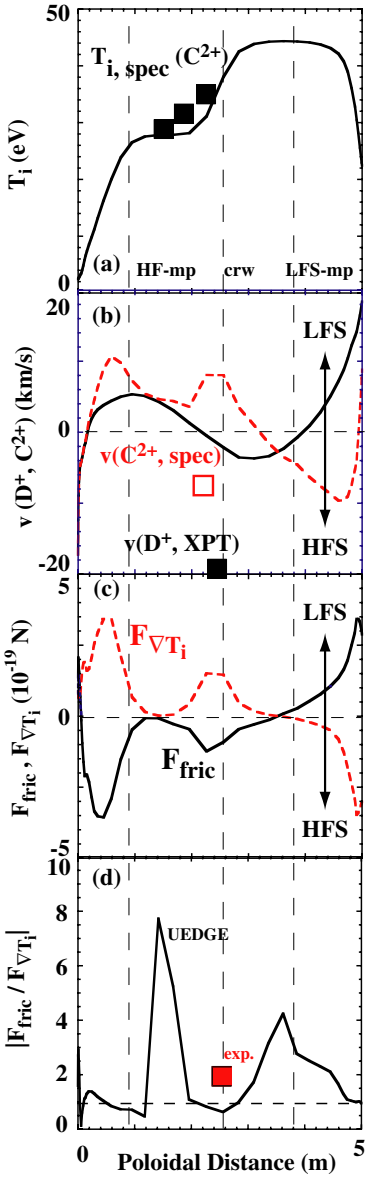

Figure 14. (*a*) Predicted poloidal profile of the ion temperature along the flux surface at distance 2 cm at the outer midplane. The measured ion temperature of C^{2+} ions from spectroscopy is shown by the black squares (DIII-D shot 133935). (*b*) Predicted poloidal profile of the deuteron (black solid line) and C^{2+} (red dashed) ion velocities along the 2 cm flux surface. Overlaid are the corresponding measured velocities from the divertor X-point reciprocating probe (from figure 2 and [34], DIII-D shot 126903, solid black square) and Doppler spectroscopy (DIII-D shot 133935, open red squares). (*c*) Predicted frictional drag (F_fric, equation (1), black solid line) and ∇T_i forces ($F_{\nabla T_\mathrm{i}}$, equation (2), red dashed line) on C^{2+} ions at the 2 cm flux surface. A negative force is in the direction of the HFS divertor. (*d*) Poloidal profile of the $F_\mathrm{fric}/F_{\nabla T_\mathrm{i}}$ ratio on C^{2+} ions along the 2 cm flux surface. The red square indicates the force ratio estimated from the data shown in (*a*) and (*b*).

deuteron flow velocities measured in the experiment, which are not reproduced in the simulations. In the USN-$V_{\nabla B\downarrow}$ case, the HFS divertor is significantly hotter than in the USN-$V_{\nabla B\uparrow}$ case, thus the ∇T_i force along the main SOL is significantly smaller. In this case the drag force exceeds the ∇T_i force at the HFS of the crown and effectively pushes C^{2+} ions towards the HFS divertor. At the LFS of the crown, both forces are

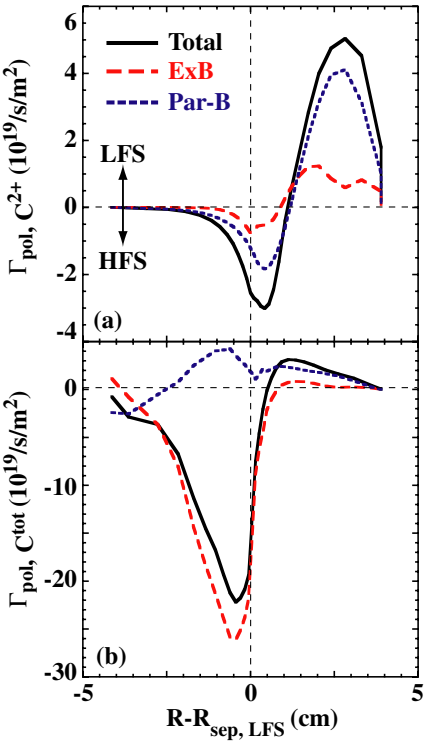

Figure 15. (*a*) The poloidal flux of C^{2+} ions separated in total (black solid line), $\boldsymbol{E} \times \boldsymbol{B}$ (red dashed) and parallel projection from the parallel flow (blue dotted). These calculations were performed for the USN-$V_{\nabla B\uparrow}$ configuration. (*b*) As (*a*) for the total poloidal carbon flux. Negative flux denotes flow towards the HFS divertor.

towards the LFS divertor producing C^{2+} flow towards the LFS divertor.

Carbon ion pressure gradient forces at the crown do not play a significant role in the simulations since the main carbon source is at the divertor target plates. This is true for simulations without and with trace carbon injection at the crown. Ion pressure gradient forces may not be excluded in the experiment as the lower divertor baffle represents the closest limiting surface in the main chamber. Spectroscopic measurements in plasmas without methane injection show that the plasma–wall interaction at the baffle is significantly lower than in the divertor. However, since the force balance at the crown is delicate, even a small carbon source may introduce a carbon pressure hill, which would induce carbon flow away from the crown towards both the HFS and the LFS divertors. Such a mechanism cannot be excluded based on the existing experimental results and simulations.

Poloidally, the simulations show that the flow of low charge-state carbon ions is dominated by the parallel flow component (C^{2+}, figure 15(*a*)). The predicted $\boldsymbol{E} \times \boldsymbol{B}$ driven flow from the simulated $\boldsymbol{E}_r$ in the far SOL is too small to play a significant role for low charge-state carbon ions (figures 12(*a*) and 15(*a*)). The $\boldsymbol{E} \times \boldsymbol{B}$ driven flow would approximately double if the measured $\boldsymbol{E}_r$ is used. However, the direction of the flow is in the direction of the LFS divertor, which is in the opposite direction as measured by spectroscopy and imaging. On the other hand, the poloidal flow of higher charge-state carbon ions carrying the bulk of the total carbon flow is determined by both the parallel-$\boldsymbol{B}$ and $\boldsymbol{E} \times \boldsymbol{B}$ components.

For the simulation of the USN-$V_{\nabla B\uparrow}$ configuration, the total poloidal carbon flux is governed by $\boldsymbol{E} \times \boldsymbol{B}$ drifts on the carbon ions in the direction of the HFS divertor in the near-separatrix part of the SOL ($0 < R - R_{\mathrm{sep,LFS}} < 0.5$ cm) (figure 15(*b*)). For $R - R_{\mathrm{sep,LFS}} > 0.5$ cm the poloidal flow is determined by the parallel-B component pointing towards the LFS divertor.

3.2. Variations of HFS divertor pumping and radial transport model

The boundary conditions for neutral pumping at the HFS target plate and the poloidal distribution of the radial fluxes have been systematically varied to investigate their effect on the simulated flow field at the crown. Increasing the neutral pumping efficiency at the HFS target plate leads to attachment of the HFS divertor plasma, and increases the magnitude of the deuteron flow at the crown towards the HFS divertor in the SOL (figures 16(*a*) and (*b*)). These simulations were performed to address the effect of detachment of the HFS divertor plasma and thus carried out for the USN-$V_{\nabla B\uparrow}$ configuration. By raising the assumed pumping efficiency uniformly across the HFS divertor plate from zero to 10%, the electron temperature at the HFS divertor plate increases from 2 to 15 eV, making the numerical solution for the HFS divertor plasma less consistent with the Langmuir probe and carbon emission profile measurements. Simultaneously, the deuteron Mach number increases from zero to 0.1 in the far SOL ($R - R_{\mathrm{sep,LFS}} = 2$ cm). At 10% pumping efficiency, the deuterons flow in the far SOL from the LFS midplane towards the HFS divertor (figure 16(*b*)). The predicted Mach number in the main SOL, including the crown is still significantly lower than the measurements (figures 2 and 16(*b*)). The predicted C^{2+} flow velocity significantly decreases at the crown, and even changes its direction in the LFS of the crown, due to the enhanced frictional drag from the deuterons and the reduction in the ∇T_{i} force (figure 16(*c*)). However, in the HFS of the crown the flow of C^{2+} remains in the direction of the LFS divertor, which is in disagreement with the measurements.

Varying the particle and thermal diffusivities poloidally as a function of $1/B_{\mathrm{T}}^{n}$, where $n = 0, 1, 2, 3$, did not result in any significant change in the directions or magnitudes of the deuteron and C^{2+} flow velocities (figures 17(*b*)–(*d*)). In going from a weakly ($n = 0$) to a more strongly ballooning-type transport model ($n = 3$), the radial diffusive flux across the separatrix at the HFS midplane was reduced by a factor of 4, while at the LFS midplane the flux was kept the same (figure 17(*a*)). The overall SOL flow pattern is only weakly affected by introducing poloidally varying diffusivities, due to the strong effect of the radial ion $\boldsymbol{B} \times \nabla B$ drift at the crown and divertor X-point. Consequently, the radial and poloidal profiles of the deuteron and C^{2+} flow velocities are similar for the four $1/B_{\mathrm{T}}$ cases investigated, and the deuteron flow velocity at the crown remains low. These results are qualitatively consistent with similar numerical studies using the UEDGE [21] and SOLPS [55] codes. In comparison with [21], significantly lower deuteron flows in the SOL were obtained in this work. The discrepancy is likely to be due to the enhanced effect of the ion $\boldsymbol{B} \times \nabla B$ drift at the crown observed in this work, when the drifts were fully turned on, while in [21] they were suppressed by 2/3.

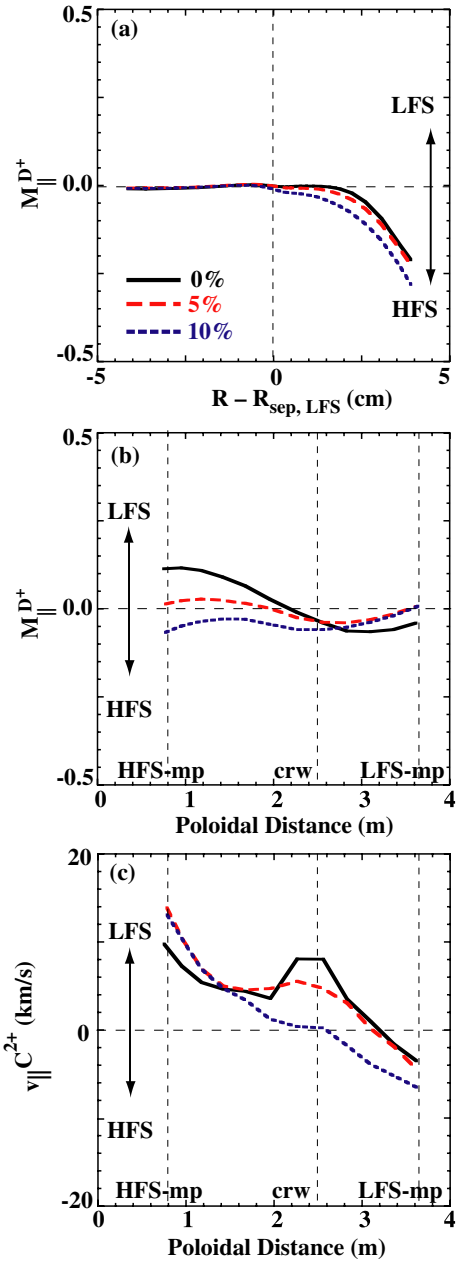

Figure 16. (*a*) Predicted radial profile of the deuteron Mach number as a function of $R - R_{\mathrm{sep,LFS}}$, (*b*) poloidal profile of the deuteron Mach from the HFS to the LFS midplane at the 2 cm flux surface and (*c*) poloidal profile of the parallel-$\boldsymbol{B}$ velocities of C^{2+} ions from the HFS to the LFS midplane at the 2 cm flux surface. UEDGE simulations for three different pumping conditions at the HFS target plate are shown: zero pumping (black solid line), 5% pumping (red dashed) and 10% pumping (blue dotted). A negative Mach number or velocity denotes motion towards the HFS divertor.

The SOL deuteron flow in the parallel-$\boldsymbol{B}$ direction integrated radially at the crown as calculated by UEDGE is 5×10^{20} particles s^{-1}, approximately one order of magnitude lower than measured with the reciprocating probe. This number can be compared with the total deuteron outflow from the core into the SOL predicted by UEDGE, which is of the order 2.5×10^{21} particles s^{-1}. Even with the assumption that the radial flux of deuteron across the separatrix is strongly peaked at the LFS midplane, as achieved by using a strongly ballooning-type transport model ($n = 3$), the simulations cannot reproduce the total deuteron throughput at the crown. Further numerical investigations are necessary to elucidate the discrepancy between the measurements and the simulations.

4. Discussion and summary

Measurements of the flow velocities of deuterons and low charge-state carbon ions (C^{1+},C^{2+}) at the crown of L-mode plasmas in DIII-D showed that carbon is not necessarily entrained in background plasma flow. Physics processes other than frictional drag must influence carbon transport in the main SOL. A possible force could be produced by the poloidal gradient in the ion temperature that was measured on C^{2+} ions at the crown, which would cause carbon ions to flow away from the divertor and towards the crown. These new results must be considered when interpreting previous carbon transport studies in DIII-D using isotopically tagged carbon (^{13}C), and they challenge our present understanding of material migration in tokamaks. The studies presented in this paper were performed in low-density, marginally collisional SOL plasmas. In configurations with the ion $\boldsymbol{B} \times \nabla B$ drift towards the X-point (USN-$V_{\nabla B\uparrow}$), the deuterons and C^{2+} ions were both found to flow towards the HFS at the HFS of the crown, albeit with different velocities. The deuterons were measured to flow at -20 to -30 km s^{-1}, the C^{2+} at -5 to -15 km s^{-1}. In the case with the ion $\boldsymbol{B} \times \nabla B$ drift away from the X-point (USN-$V_{\nabla B\downarrow}$), the deuteron flow is zero, but carbon ions flow at -5 to -15 km s^{-1} towards the HFS divertor. Poloidally, the C^{1+} velocities at the HFS were measured to be consistent with parallel-$\boldsymbol{B}$ motion; imaging would suggest that the $\boldsymbol{E} \times \boldsymbol{B}$ flow component is small compared with the poloidal projection of parallel-$\boldsymbol{B}$ flow.

Plasma simulations with the multi-fluid edge code UEDGE predict significantly lower deuteron and C^{2+} flow velocities than measured in the USN-$V_{\nabla B\uparrow}$ configuration. The simulations include the cross-field terms due to $\boldsymbol{E} \times \boldsymbol{B}$ and $\boldsymbol{B} \times \nabla B$. While including these terms does not significantly change the predicted flow fields in the vicinity at the crown, their inclusion does produce plasma solutions in the divertor that are more consistent with measurements than simulations without them, but complete agreement with the measurements in the divertor is yet to be obtained. The simulations indicate that the deuteron flow along $\boldsymbol{B}$ is determined by pressure imbalance between the divertor X-point and the crown: due to the $\boldsymbol{B} \times \nabla B$ drift the crown is either a pressure sink (USN-$V_{\nabla B\uparrow}$) or a pressure hill (USN-$V_{\nabla B\downarrow}$). Consequently, in the former case, the SOL flow is predominately from the X-point to the crown, in the latter case from the crown towards the X-point, consistent with Pfirsch–Schlüter driven flow [20, 52, 53]. The simulations also show the transport of low-charge state carbon ions in the main SOL is determined mainly by electrostatic coupling to the deuterons and the ion temperature gradient force. A poloidally peaked ion temperature profile is predicted by UEDGE, with its maximum at the LFS midplane, pushing carbon ions from the HFS X-point towards the crown. Depending on the direction of the deuteron flow in the vicinity of the crown, C^{2+} ions are predicted to flow either towards the LFS divertor

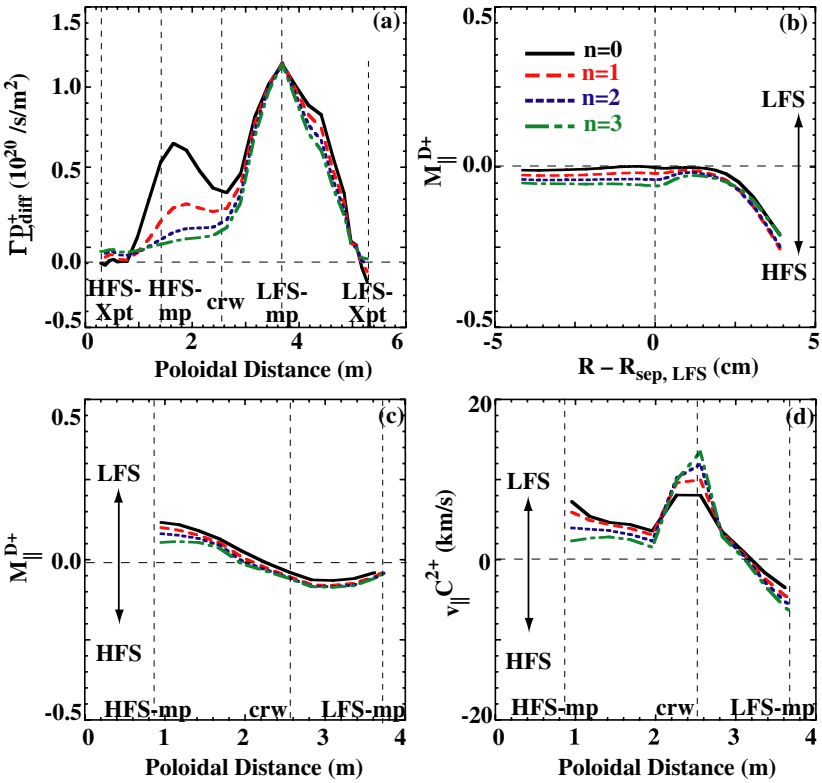

Figure 17. (*a*) Predicted poloidal profile of the deuteron flux due to diffusion only from the HFS to the LFS X-point, (*b*) radial profile of the deuteron Mach number as a function of $R - R_{\mathrm{sep,LFS}}$ number as a function of $R - R_{\mathrm{sep,LFS}}$, (*c*) poloidal profile of the deuteron Mach from the HFS to the LFS midplane at the 2 cm flux surface and (*d*) poloidal profile of the parallel-$\boldsymbol{B}$ velocities of C^{2+} ions from the HFS to the LFS midplane at the 2 cm flux surface. UEDGE simulations for four different assumptions on the poloidal distribution of radial diffusivities ($\sim 1/B_{\mathrm{T}}^{n}$) are shown: $n = 0$ (black solid line), $n = 1$ (red dashed), $n = 2$ (blue dotted) and $n = 3$ (green dashed−dotted). A negative Mach number or velocity denotes motion towards the HFS divertor.

only (USN-$V_{\nabla B\uparrow}$) or towards the HFS and LFS divertors from their respective sides of the crown (USN-$V_{\nabla B\downarrow}$). The predicted velocity difference between the deuterons and C^{2+} ions is of the same order of magnitude as the measured difference. Assuming that the velocity difference remains the same, an increase in the deuteron velocity towards the HFS divertor in the simulations would result in an increase in the flow velocity of C^{2+} ions in the same direction. The simulations appear to capture the flow of carbon ions, but not so the flow of the deuterons. Increasing the assumed pumping efficiency at the HFS divertor target in the simulations increases the deuteron flow velocity at the crown, but moves the plasma solutions obtained in the HFS divertor away from the measurements. Varying the particle and thermal diffusivities poloidally as an inverse function of toroidal magnetic field does not significantly change the radial and poloidal profiles of the deuteron and C^{2+} flow velocities. The simulations generally show that the flow pattern in the SOL is determined mainly by cross-field, ion $\boldsymbol{B} \times \nabla B$ drifts between the crown and the divertor X-point and a corresponding return flow parallel to $\boldsymbol{B}$ in the SOL. Kinetic effects due to ion orbit losses across the separatrix may play a role in driving flows in the SOL; their effect is yet to be studied.

Acknowledgment

This work performed under the auspices of the US Department of Energy by the Lawrence Livermore National Laboratory under Contract DE-AC52-07NA27344, DE-FG02-07ER54917, DE-FC02-04ER54698, DE-AC05-00OR22725, DE-AC04-94AL85000 and DE-FG02-08ER54984.

References

[1] Matthews G.F. 2005 *J. Nucl. Mater.* **337–339** 1
[2] Pitts R.A. *et al* 2005 *Plasma Phys. Control. Fusion* **47** B303
[3] Loarte A. *et al* 2007 *Nucl. Fusion* **47** S203
[4] Lipschultz B. *et al* 2007 *Nucl. Fusion* **47** 1189
[5] Boedo J.A., Schaffer M.J., Maingi R. and Lasnier C.J. 2000 *Phys. Plasmas* **7** 1075
[6] Petrie T.W. *et al* 2006 *Nucl. Fusion* **46** 57
[7] Isler R.C., Brooks N.H., West W.P., Porter G.D. and the DIII-D Divertor Team 1999 *Phys. Plasmas* **6** 1837
[8] Groth M. *et al* 2007 *Phys. Plasmas* **14** 056120
[9] Erents S.K. *et al* 2000 *Plasma Phys. Control. Fusion* **42** 905
[10] Gunn J.P. *et al* 2007 *J. Nucl. Mater.* **363–365** 484
[11] Asakura N. and the ITPA SOL and Divertor Topical Group 2007 *J. Nucl. Mater.* **363–365** 41
[12] Jablonski D., LaBombard B., McCracken G.M., Lisgo S., Lipschultz B., Hutchinson I H., Terry J. and Stangeby P.C. 1997 *J. Nucl. Mater.* **241–243** 782
[13] McLean A.G. *et al* 2005 *J. Nucl. Mater.* **337–339** 124
[14] Stangeby P.C. *et al* 2003 *J. Nucl. Mater.* **313–316** 883
[15] Chankin A.V. *et al* 1996 *Plasma Phys. Control. Fusion* **38** 1579
[16] Porter G.D., Isler R., Boedo J. and Rognlien T.D. 2000 *Phys. Plasmas* **7** 3663
[17] Groth M. *et al* 2005 *J. Nucl. Mater.* **337–339** 425

[18] Erents S.K. *et al* 2004 *Plasma Phys. Control. Fusion* **46** 1757
[19] Porter G.D., Rognlien T.D., Rensink M.E., Wolf N.S. and West W.P. 2001 *J. Nucl. Mater.* **290–293** 692
[20] Chankin A.V., Corrigan G., Erents S.K., Matthews G.F., Spence J. and Stangeby P.C. 2001 *J. Nucl. Mater.* **290–293** 518
[21] Pigarov A.Yu., Krasheninnikov S.I., LaBombard B. and Rognlien T.D. 2008 *Contrib. Plasma Phys.* **48** 82
[22] Rozhansky V.A., Molchanov P.A., Voskoboynikov S.P., Counsell G., Kirk A., Coster D.P. and Schneider R. 2007 *J. Nucl. Mater.* **363–365** 664
[23] Molchanov P.A., Rozhansky V.A., Voskoboynikov S.P., Tallents S., Counsell G. and Kirk A. 2008 *Plasma Phys. Control. Fusion* **50** 115010
[24] Chankin A.V. *et al* 2007 *Nucl. Fusion* **47** 762
[25] Chankin A.V. *et al* 2009 *Nucl. Fusion* **49** 015004
[26] Rognlien T.D., Milovich J.L., Rensink M.E. and Porter G.D. 1992 *J. Nucl. Mater.* **196–198** 347
[27] Groth M. *et al* 2009 *J. Nucl. Mater.* **390–391** 343
[28] Wampler W.R., McLean A.G., Allen S.L., Brooks N.H., Elder J.D., Fenstermacher M.E., Groth M., Stangeby P.C., West W.P. and Whyte D.G. 2007 *J. Nucl. Mater.* **363–365** 72
[29] Greenwald M. *et al* 1988 *Nucl. Fusion* **28** 2199
[30] Carlstrom T.N. *et al* 1992 *Rev. Sci. Instrum.* **63** 4901
[31] Watkins J.G. *et al* 1992 *Rev. Sci. Instrum.* **63** 4728
[32] Burrell K.H. 2001 *Rev. Sci. Instrum.* **72** 1023
[33] Stangeby P.C. 2000 *The Plasma Boundary of Magnetic Fusion Devices* (Bristol: Institute of Physics Publishing)
[34] Watkins J.G. *et al* 1997 *Rev. Sci. Instrum.* **68** 373
[35] Brooks N.H. *et al* 1992 *Rev. Sci. Instrum.* **63** 5167
[36] Fenstermacher M.E., Meyer W.H., Wood R.D., Nilson D.G., Ellis R. and Brooks N.H. 1997 *Rev. Sci. Instrum.* **70** 974
[37] Hutchinson I.H. 1988 *Phys. Rev.* A **37** 4358
[38] Moyer R.A. *et al* 1995 *Phys. Plasmas* **2** 2397
[39] Kočan M. *et al* 2008 *Rev. Sci. Instrum.* **50** 125009
[40] Carlstrom T.N., Hsieh C.L., Stockdale R., Nilson D.G. and Hill D.N. 1997 *Rev. Sci. Instrum.* **68** 1195
[41] Zeng L., Doyle E.J., Luce T.C. and Peebles W.A. 2001 *Rev. Sci. Instrum.* **72** 320
[42] Watkins J.G., Moyer R.A., Cuthbertson J.W., Buchenauer D.A., Carlstrom T.N., Hill D.N. and Ulrickson M. 1997 *J. Nucl. Mater.* **241–243** 645
[43] Boedo J.A. 2009 *J. Nucl. Mater.* **390–391** 29
[44] Spitzer L. 1962 *Physics of Fully Ionized Gases* 2nd edn (New York: Wiley)
[45] Lao L.L. *et al Nucl. Fusion* **25** 1611
[46] Rognlien T.D., Poter T.D. and Ryutov D.D. 1999 *J. Nucl. Mater.* **266–269** 654
[47] Davis J.W., Haasz A.A. 1997 *J. Nucl. Mater.* **241–243** 37
[48] Neuhauser J. *et al* 1984 *Nucl. Fusion* **24** 39
[49] ADAS Atomic Data and Analysis Structure 1995–2008 *ADAS News* The ADAS Project, http://adas.phys.strath.ac.uk
[50] Boedo J.A., Porter G.D., Schaffer M.J., Lehmer R., Moyer R.A., Watkins J.G., Evans T.E., Lasnier C.J., Leonard A.W. and Allen S.L. 1998 *Phys. Plasmas* **5** 4305
[51] Fenstermacher M.E. *et al* 1997 *Phys. Plasmas* **4** 1761
[52] Asakura N. *et al* 2000 *Phys. Rev. Lett.* **84** 3093
[53] Pitts R.A. *et al* 2007 *J. Nucl. Mater.* **363–365** 505
[54] Rozhansky V.A. *et al* 2001 *Nucl. Fusion* **41** 387
[55] Coster D.P. *et al* 2004 Integrated modelling of material migration and target plate power handling at JET *Proc. 20th Int. Conf. Fusion Energy 2004 (Vilamoura, Portugal, 2004)* (Vienna: IAEA) CD-ROM file TH/P5-18 and http://www-naweb.iaea.org/napc/physics/fec/fec2004/datasets/index.html